

References: Archer, M.A., J.P. Phelan, K.A. Beckman, and M.R. Rose 2003, *Evolution* 60: 1435–1444; Ballard, J.W.O., R.G. Melvin, and S.J. Simpson 2008, *Journal of Insect Physiology* 54: 1371–1376; Bock, I.R., and M.R. Wheeler 1972, *University of Texas Publ.* 7213: 1–102; Boucher, L., and J. Huignard 1987, *Journal of Insect Physiology* 33: 949–957; Brandy, R., S. Sarah, B. Jessica, R. Robin, W. Michael, and G. Jadwiga 2007, *Aging Cell* 6: 723–726; Butlin, R.K., C.W. Woodhatch, and G.M. Hewitt 1987, *Evolution* 41: 221–225; Chapman, T., L.F. Liddle, J.M. Kalb, M.F. Wolfner, and L. Partridge 1995, *Nature* 373: 241–244; Chapman, T., and S.J. Davies 2004, *Peptides* 25: 1477–1490; Chippindale, A.K., T.J.F. Chu, and M.R. Rose 1996, *Evolution* 50: 753–766; Chippindale, A.K., A.G. Gibbs, M. Sheik, K.J. Yee, M. Djawdan, T.J. Bradley, and M.R. Rose 1998, *Evolution* 52: 1342–1352; Djawdan, M., A.K. Chippindale, M.R. Rose, and T.J. Bradley 1998, *Physiological Zoology* 71: 584–594; Edvardsson, M., 2006, *Animal Behaviour* 74: 183–188; Graves, J.L., E.C. Toolson, C. Jeong, L.N. Vu, and M.R. Rose 1992, *Physiological Zoology* 65: 268–286; Gupta, J.P., and K.K. Panigrahy 1990, *Genetica* 82: 45–49; Harshman, L.G., and J.L. Schmid 1998, *Evolution* 52: 1679–1685; Harshman, L.G., K.M. Moore, M.A. Sty, and M.M. Magwire 1999, *Neurobiology of Aging* 20: 521–529; Hoffmann, A.A., and L.G. Harshman 1999, *Heredity* 83: 637–643; Hoffmann, A.A., R. Hallas, A.R. Anderson, and M. Telonis-Scott 2005, *Journal of Evolutionary Biology* 18: 804–810; Hoffmann, A.A., and P.A. Parsons 1993, *Biological Journal of the Linnean Society* 48: 43–54; Ivy, T.M., J.C. Johnson, and S.K. Sakaluk 1999, *Proc. Roy. Soc. B* 266: 1523–1527; Koehn, R.K., and B.L. Bayne 1989, *Biol. J. Linn. Soc.* 37: 157–171; Knowles, L.L., B.B. Hernandez, and T.A. Markow 2004, *Proc. Roy. Soc. B* 271(Suppl 5): S357–S359; Knowles, L.L., B.B. Hernandez, and T.A. Markow 2005, *J. Evol. Biol.* 18: 156–161; Luciano, M.M., D.W. Thomas, and A.M. Therese 2009, *Functional Ecology* 23: 521–527; Lung, O., U. Tram, C.M. Finnerty, M.A. Eipper-Mains, J.M. Kalb, and M.F. Wolfner 2002, *Genetics* 160: 211–224; Medina-Navarro, R., G. Durán-Reyes, M. Díaz-Flores, and C. Vilar-Rojas 2010, *PLoS ONE* 5(1): 1–11; Randall, D., W. Burggren, and K. French 1997, *W.H. Freeman and Company* (4), New York; Rego, C., M.R. Rose, and M. Matos 2007, *Physiological and Biochemical Zoology* 80: 347–357; Rion, S., and T.J. Kawecki 2007, *Journal of Evolutionary Biology* 20: 1655–1664; Rose, M.R., L.N. Vu, S.U. Park, and J.L. Graves, Jr. 1992, *Experimental Gerontol.* 27: 241–250; Rose, M.R., and M.A. Archer 1996, *Current Opinion in Genetics and Development* 6: 366–370; Service, P.M., E.W. Hutchinson, M.D. Mackinley, and M.R. Rose 1985, *Physiological Zoology* 58: 380–389; Tapiwanashe, M., W. Melanie, R. Kumars, P.M. Michael, A.J. Robin, and L.P. Smith 2006, [Mechanisms of Ageing and Development](#) 127 (4): 356–370; Wolfner, M.F., 1997, *Insect Biochem. Molec. Biol.* 27: 179–192; Wolfner, M.F. 2002, *Heredity* 88: 85–93.



### Quantitative assessment of ommatidial distortion in *Drosophila melanogaster*.

**Caudron, Quentin,<sup>1</sup> Ceri Lyn-Adams,<sup>2,5</sup> John A.D. Aston,<sup>3</sup> Bruno G. Frenguelli,<sup>2</sup> and Kevin G. Moffat.<sup>2</sup>**

<sup>1</sup>Department of Ecology and Evolutionary Biology, Princeton University, Princeton, NJ, 08542, USA; <sup>2</sup>School of Life Sciences, University of Warwick, Coventry, CV4 7AL, UK; <sup>3</sup>CRiSM, Department of Statistics, University of Warwick, Coventry, CV4 7AL, UK; <sup>5</sup>Current affiliation: BBSRC, Polaris House, North Star Avenue, Swindon, Wiltshire, SN2 1UH, UK.

Assessing the structural characteristics of an organism's physical appearance can be an important aspect of evaluating the effect of protein-protein interactions. Many biomedical

applications require the extraction of structural features from images, in order to infer information about the underlying biological processes causing a phenotype. This is typically arduous and subject to human bias. A general methodology for extracting structural information from images using edge detection and boundary-walking algorithms is presented. This yields quantitative descriptors and comparators of disorder, applied to the problem of unambiguous identification of phenotypic alterations induced by *tau*-dependent neurodegeneration in the adult eye of *Drosophila melanogaster*. This method obviates traditional subjective assessment techniques, enabling quantitative tests of the influence of genetic interactions on *Drosophila* phenotypes. Using this framework, we quantify from images of *Drosophila* eyes, a coefficient of distortion for a number of genotypes, and demonstrate that subtle changes in phenotype are detectable, allowing the direct numerical comparison between the extent of distortion.

## Introduction

A major challenge in neurodegenerative disease research is obtaining information regarding interactions within cellular signaling networks. Model organisms such as *Drosophila melanogaster* can be used to study these networks, either through the insertion of relevant human genes, or their homologues, into the model organism's genome (Bilen and Bonini, 2005) or the mutation of endogenous genes (St. Johnston, 2002). These genetic alterations can result in changes in the morphology of structures within the organism, which are then used as convenient and experimentally tractable surrogates for manipulations in mammalian models. However, when these morphological changes are captured in images, difficulties arise in identifying and isolating the structural features present in order to quantitatively assess their deviation from the norm.

The *Drosophila* eye is frequently used as a model in developmental and neurodegenerative disease research due to its very regular morphology (Lu and Vogel, 2009). The fly's compound eye is comprised of approximately 700 to 800 individual ommatidia, displaying ordered hexagonal packing, and each containing a cluster of neurons (Moses, 2002). Human Tau protein can be expressed in *Drosophila* in order to study its interaction with other candidate proteins implicated in tauopathies such as Alzheimer's disease. Expression of human *tau* is toxic to developing eye cells, resulting in distortion of the ommatidial lattice (*e.g.*, Iijima-Ando and Iijima, 2010) through fusion of ommatidia, loss of regularity of the hexagonal lattice, and a decrease in ommatidia count and eye size (Chatterjee *et al.*, 2009).

Currently, *Drosophila* biologists often apply qualitative judgment to describe the extent to which disorder is visible in the eye, with terms such as “better” or “slightly rougher” qualifying any differences between samples; even unofficial grading systems, if present, are purely subjective (Muraro and Moffat, 2006). Recent work has tried to introduce a more quantitative version of visual inspection using rating scales (Pandey *et al.*, 2007), but these are also subjective in the weight that is given to each rating. Others have focused on the packing expected in the *Drosophila* pupal eye ommatidia, measuring defects in the expected hexagonal lattice (Johnson and Cagan, 2009). This methodology, however, retains subjective weighting by failing to account for the severity of observed defects and requires the data to be hand-processed, introducing possible human error. Yet another approach focused on calculating the volume occupied by the eye, a method which may overlook the small-scale detail present in the ommatidia (Ambegaokar and Jackson, 2010).

A framework for the extraction of information from biomedical images and for direct comparison between physical attributes is presented, specifically applied to the measurement of the distortion present in the *Drosophila* eye phenotype as a result of Alzheimer's disease-related gene expression, in this case, human *ON4R tau* and *Drosophila shaggy*, a *GSK3-β* homologue. The

methodology is demonstrated to quantify and statistically test the effect of gene interactions within the *tau* regulatory network. This framework is adaptable to other areas of the fly, such as the wing, and indeed other organisms, as in the phenotypic changes seen in Parkinson's disease research in *Caenorhabditis elegans* (Buckingham and Sattelle, 2008) or in cancer screening in human blood samples (Zhang, Wang, and Qi, 2006). The implementation of the algorithm is available freely as source code online, as QED (<http://github.com/QCaudron/QED>).

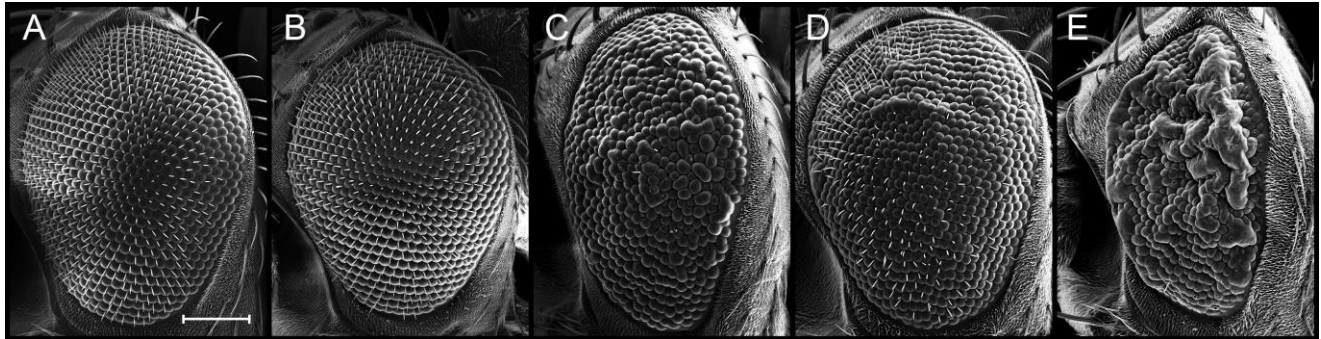


Figure 1. Example images representing the five genotypes compared in this work. Image A shows the wild type CS eye, B shows the  $GMR::GAL4$  control, C shows  $GMR>tau$ , D shows  $GMR>sgg$ , and E shows the strain expressing both *tau* and *sgg* transgenes,  $GMR>tau>sgg$ . The scale bar, measuring 100  $\mu m$ , applies to all images.

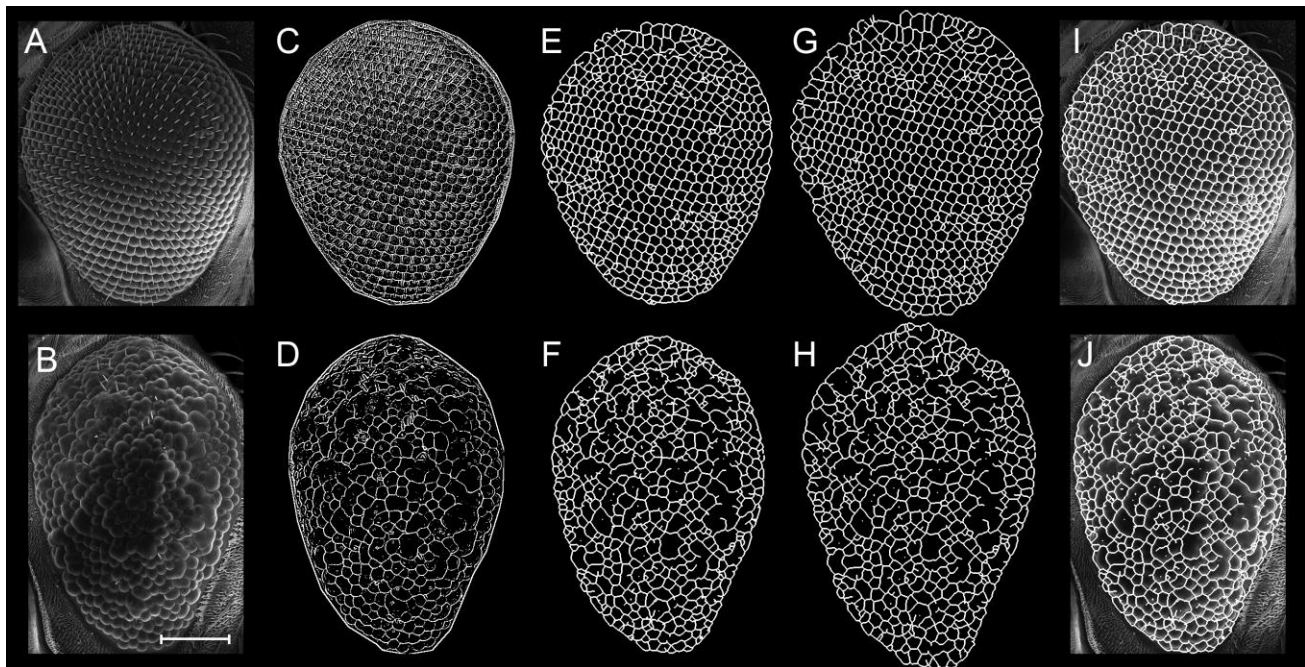


Figure 2. The progression of the edge detection framework on a  $GMR$  control eye (top row) and on a  $GMR>tau$  eye (bottom row). A-B show the original images; C-D have been masked around the eye and had the *PLUS* edge detection method applied; E-F show the edges after Sobel edge detection and morphological dilation and thinning; G-H show the edgeset after its perspective transform; I-J detail the final edgeset superimposed onto the original image, for comparison. The scale bar applies to all images, and measures 100  $\mu m$ .

## Results

Example images of the five genotypes used can be seen in Figure 1.

Figure 2 shows the QED methodology applied to images of a GMR control eye (2A) and of a *GMR>tau* eye (1B). Results of the first pass of edge detection algorithms are presented in Figure 2C-D, and after final edge detection and edgeset reconstruction in 2E-F. Figure 2G-H show the edgeset after its perspective transform. Here the outer regions of the eye were enlarged to compensate for the curvature of the eye. Figure 2I-J show the edgeset before its perspective transform, superimposed onto the image of the eye.

Figure 3 presents the cumulative distributions of distortion coefficients for the five genotypes, showing all distributions to be distinct. The number of samples, mean roundness coefficients  $\bar{\Delta}_R$  and *p*-values for tests against the control genotype are shown in Table 1.

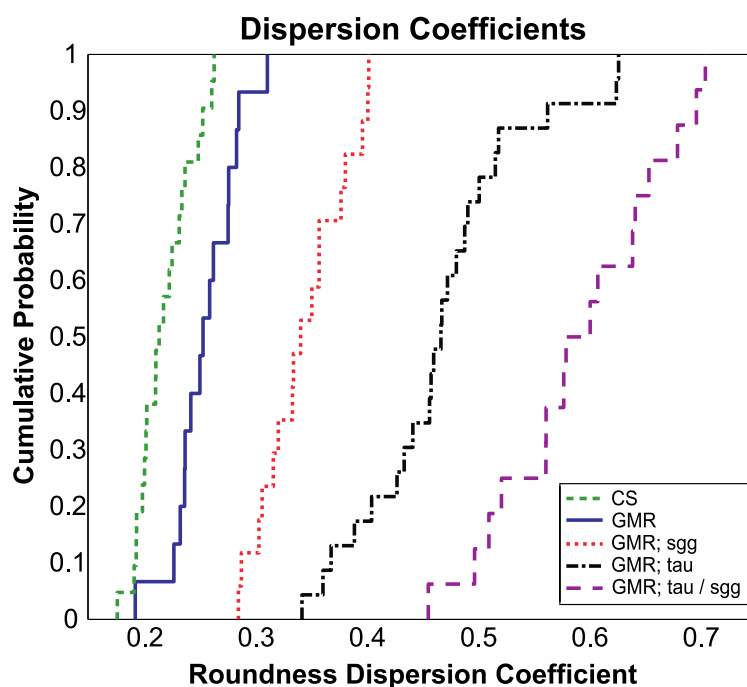


Figure 3. The cumulative distributions of roundness coefficients for all five genotypes. The wild type (CS) flies (green line) have the lowest average roundness coefficient, and hence the least variation in the shape of their ommatidia, followed by the GMR control genotype (blue line). The *GMR>tau>sgg* genotype (purple line) shows the most variation in roundness, worse than when *tau* is expressed alone (black line). The *GMR>sgg* genotype (red line) lies in the middle, showing clear signs of toxicity, but much less than *GMR>tau* or *GMR>tau>sgg* flies.

Table 1. Number of images for each genotype *N*; mean roundness distortion coefficient  $\bar{\Delta}_R$ ; and *p*-values of the comparisons between the different genotypes.

Genotype	<i>N</i>	$\bar{\Delta}_R$	$P_{GMR}$	$P_{GMR; \tau}$	$P_{GMR; sgg}$
CS	21	0.219	$8.47 \times 10^{-4}$		
GMR :: GAL4	15	0.255			
GMR > <i>tau</i>	23	0.470	$2.80 \times 10^{-7}$		
GMR > <i>sgg</i>	17	0.345	$4.08 \times 10^{-6}$	$9.71 \times 10^{-7}$	
GMR > <i>tau</i> > <i>sgg</i>	16	0.593	$2.32 \times 10^{-6}$	$6.03 \times 10^{-5}$	$1.06 \times 10^{-6}$

Visually, it is clear that the *GMR>tau>sgg* eyes were the most distorted, showing very pronounced ommatidial fusion and large-scale warping of the surface of the eye along with complete loss of bristles. The very large mean distortion coefficient  $\bar{\Delta}_R$  for this genotype reflects the distortion

present in this genotype. The extent of the distortion in GMR>tau>sgg was found to be significantly different ( $p = 6.03 \times 10^{-5}$  or smaller) to the distortion of other genotypes.

Ommatidial fusion was evident on GMR>tau eyes, though on a much smaller scale, and the surface showed significantly less distortion than in GMR>tau>sgg eyes, as is evident by the mean distortion coefficient  $\bar{\Delta}_R = 0.470$  being significantly smaller when compared with those of GMR>tau>sgg ( $\bar{\Delta}_R = 0.593, p = 6.03 \times 10^{-5}$ ), but significantly larger than those of the control genotype, GMR::GAL4 ( $\bar{\Delta}_R = 0.255, p = 2.32 \times 10^{-6}$ ).

GMR>sgg eyes were found to be less distorted than GMR>tau or GMR>tau>sgg eyes, with a mean distortion coefficient of  $\bar{\Delta}_R = 0.345$ . Visually, the most obvious defects are weak ommatidial fusion and a slight disordering of the hexagonal lattice. The distortion coefficients were noted to be significantly different to those of other genotypes.

GMR::GAL4 eyes could not consistently be distinguished from wild type (CS) eyes by visual inspection. Analysis, however, yields a significant difference ( $p = 8.47 \times 10^{-4}$ ), identifying GMR::GAL4 eyes as being more distorted with a mean distortion coefficient of  $\bar{\Delta}_R = 0.255$  compared with  $\bar{\Delta}_R = 0.219$  for CS, implying that the GMR::GAL4 control eyes display a weak phenotypic distortion.

## Discussion

These results confirm the ability of the QED methodology to statistically quantify the effects of genetic interactions, thereby eliminating subjectivity in the analysis of structural phenotypes. Moreover, it allows subtle changes in phenotype to be unambiguously determined, as evidenced by the comparison of CS and GMR::GAL4 flies. QED also provides quantitative descriptions of the relative phenotypic differences.

The modular approach allows specialized measures of distortion to be constructed to fit a specific function, allowing for a wide scope of operation. By tailoring the measures to the problem, a considerable amount of information can be extracted from images and normalized to allow for comparison by the statistical processes described.

This methodology can be expected to contribute significantly to fields where visual analysis is the current *modus operandi*, such as in neurodegenerative disease research as exemplified here, but also in biomedical scanning procedures such as screening for abnormally-shaped cells in cancer detection or identification of anomalous structural features or growths in tissue.

## Materials and Methods

### *Drosophila melanogaster* Stocks and Imaging

The eye-specific glass multiple repeat (GMR::GAL4) driver (Ellis, O'Neil, and Rubin, 1993; Brand and Perrimon, 1993) was used for expression of a constitutively-active *Drosophila shaggy* kinase (UAS-sgg S9A; Bourouis, 2002; Chatterjee *et al.*, 2009), the ON4R isoform of human *tau* (Wittmann *et al.*, 2001), or both transgenes in combination. Flies expressing the GMR driver alone were used as controls. All genetic combinations were hemizygous for the transgenes. In addition, wild-type flies of the Canton-S strain were imaged.

Female flies were fixed overnight in 4% paraformaldehyde at 4°C. Flies were then dehydrated using an acetone series (10%, 30%, 50%, 70%, 90%), incubated on a rotator in 1 ml of solution for fifteen minutes at room temperature. Flies were then transferred to 100% acetone stored

over a molecular sieve for at least two days at 4°C. Flies were attached to stubs using double-sided tape, sputter-coated in gold for sixty seconds and imaged using a Zeiss Supra55 VP scanning electron microscope, by secondary electron detection. Each image was taken at 150× magnification at a resolution of 1024 × 768 pixels, with each pixel representing an area of 0.54 μm<sup>2</sup>. Images were saved as single-channel, 8-bit, uncompressed TIFF files. Figure 1A shows an example SEM image of the GMR genotype, and Figure 1B shows one from the GMR; tau genotype.

UAS-*sgg* S9A and GMR::GAL4 were obtained from the Bloomington Stock Center (stock numbers 5255 and 1104, respectively) and UAS-0N4R *tau* flies were supplied by Prof. Mel Feany, of Harvard Medical School.

### *Edge Detection*

Images were masked such that only the eye region remained, and all surrounding information had its pixel intensity values set to zero (black). The image was then cropped closely in both *x* and *y* directions to contain the eye region as tightly as possible.

Contrast was enhanced where required by contrast-limited adaptive histogram equalization (Zuiderveld, 1994). The image is partitioned into 8 × 8 tiles, each of which has their histograms adjusted to approximate a uniform distribution. The tiles are then recombined using bilinear interpolation to ensure artificially-induced boundaries are removed.

In gray scale images, the edges of physical objects appear as sharp changes in pixel intensity values. Because edges occur over a wide range of scales, we seek a filter that is band-limited in the frequency domain, thereby also reducing sensitivity to noise. In order to accurately localize the edges in space, our filter should also be applied to a smooth local average of pixels, and so should be band-limited in space. The distribution that minimizes the product of spatial and frequency variances, and hence optimizes these constraints, is the Gaussian distribution (Basu, 2002). Edges can then be sought in the maxima or minima of the derivative of the filtered image, or equivalently, in the zero-crossings of the second derivative. The direction in which the second-derivative is taken affects the measured magnitude of a zero-crossing and will be at a maximum in the direction normal to the edge. The second derivative of the Gaussian-filtered images is, therefore, taken as a combination of the second derivative in the gradient direction (SDGD) and the linear Laplacian, an orientation-independent second derivative operator. The resulting edge detector, *PLUS* (Verbeek and van Vliet, 1994), is more accurate by an order of magnitude than its components, the SDGD and Laplacian filters. A simplification in the implementation of *PLUS* saves on computation time by convolving the image with second derivatives of Gaussians instead of taking the second derivative of the Gaussian-convolved image; this is equivalent by convolution theory.

*PLUS* edge detection was complemented by convolution with a simple Sobel filter (Sobel and Feldman, 1973), the kernels of which approximate a first derivative of Gaussian independently in both *x* and *y* directions at each pixel. Due to the *PLUS* filtering, edges are now trivial to detect, and a threshold  $\epsilon$  easily set, returning a 1-bit (binary) image where each pixel is either black (no edge) or white (edge). The resulting image contains disconnections in the edgeset, but less noise than in the *PLUS* image, and with edges localized on the boundaries of the thicker *PLUS* edges, leading to hollowed edge sections.

A morphological dilation algorithm (Gonzalez and Woods, 1992) was applied to the edgeset image, where all white pixels had their 3 × 3 environment made white. This algorithm was run twice sequentially, effectively reconnecting broken clusters and filling out the hollow edgesets, especially in the bristles. The opposite algorithm, a morphological thinning, was then applied, removing pixels on the outer regions of thick segments until only the central pixel remained. This shrinks the thick

edges to minimally-connected strokes, and strongly reduces the appearance of bristles, both in thickness and in length. The edgeset is now of single-pixel thickness and fully connected.

Scanning electron microscopy images are two-dimensional representations of three-dimensional objects. The curvature of the eye leads to distortion in the information captured by the image, especially visible in the outer regions of the eye, where ommatidia are, pixel for pixel, smaller and less round than those in the center.

It is assumed that the curvature is hemiellipsoidal and hence convex, and that the depth of curvature ( $z$ -axis) is determined by the ( $x$ ,  $y$ ) dimensions of the eye:

$$z = \left\| \sqrt{c^2 \left[ 1 - \left(\frac{x}{a}\right)^2 - \left(\frac{y}{a}\right)^2 \right]} \right\|$$

A further assumption is made in relation to the different characteristic curvatures of various eye phenotypes: an approximation was made whereby the curvature of any eye was taken to be similarly-parameterized as that of the wild-type eye. SEM images were taken at various orientations to calculate the average polar radius  $c$  of the wild-type eye, in order to compensate for the spatial distortions obtained in SEM images. The curvature was, therefore, parameterized empirically at  $c = 0.4865$ , and a hemiellipsoidal surface was created for each image with this same radius of curvature. The equatorial radii,  $a$  and  $b$ , were defined as half of the  $x$  and  $y$  dimension of the eye, respectively, leading to a perfect half-ellipsoid.

The image was projected orthographically onto the curved surface (Maynard, 2005). This projection maps each pixel from the planar image onto a corresponding pixel on the curved surface. The projection angle is normal to the surface of the plane at all points, or equivalently, the center of focus lies at infinity.

The curved image, lying on a hemiellipsoidal surface approximating the curvature of the fly eye, was projected back onto a plane azimuthally via a vertical perspective projection. The center of focus is now a finite distance away, and the projection maps each pixel from the hemiellipsoid onto a larger plane. This induces distortions in the form of exaggerated lengths and areas, but preserves angles. Distortions are greatest on the outer regions of the eye, reducing to no exaggeration at the center of the image. This simulates an “unfolding” of the curved surface onto a plane, and compensates for the outer regions of the original image being smaller than those in the center, due to the angle of capture. Extra pixels on the larger surface were given a luminosity value of zero (black), and edgesets were reconnected by applying one morphological dilation and thinning cycle as described above.

### Information Extraction

Let  $\mathcal{O}$ , a family of sets indexed  $\{O_j\}_{j=1}^N$ , describe all of the ommatidia in an image. We define  $b_i$  as the  $i$ th (background) pixel inside a particular ommatidium. The set  $B_j = \{b_1, \dots, b_{A_j}\}$  is the set of all pixels inside a specific ommatidium  $O_j$ , with  $A_j$  being the total number of pixels forming the area inside  $O_j$ . These pixels appear as black pixels in the binary edgeset image.

We further define  $f_i$  as a (foreground) edge pixel, contained in the set of all edge pixels  $F_j = \{f_1, \dots, f_{L_j}\}$  that define ommatidium  $O_j$ , where  $L_j$  is the number of pixels forming the length of the boundary around  $O_j$ .

Each ommatidium consists of the union of its background and foreground pixels, that is,  $O_j = B_j \cup F_j$  where  $B_j \cap F_j = \emptyset \quad \forall O_j \in \mathcal{O}$ .

Boundaries  $F_j$  were found using a Moore-neighbor tracing algorithm modified by using Jacob's stopping criterion (Gonzalez, Woods, and Eddins, 2004). Individual ommatidia were isolated, allowing the calculation of their perimeters  $L_j$  and areas  $A_j$ . Any boundaries with perimeter  $L_j > 1000$  pixels were removed, being either open boundaries or the outline of the compound eye. Likewise, any boundaries with perimeter  $L_j < 50$  pixels were eliminated as erroneous measurements caused by noise or bisection of ommatidia by bristles.

Even with hexagonal packing, individual ommatidia in the wild-type eye should have regular, mostly-circular contours. A dimensionless measure of roundness of ommatidia was based on the idea that circular objects maximize their area-to-perimeter ratios. This measure is defined for each  $O_j$  as

$$R_j = 4\pi \frac{A_j}{L_j^2} \in (0, 1),$$

where a higher value of  $R_j$  indicates a rounder ommatidial shape.

Distributions of roundness measures for each image were characterized by a percentile coefficient of distortion, defined as the difference between the ninety-fifth and the fifth percentile, normalized by their sum:

$$\Delta = \frac{p_{95} - p_5}{p_{95} + p_5}.$$

This measure of distortion attempts to capture the width of the distribution, and thereby the variability present in each eye, while excluding any outliers caused by errors in edge detection, hence a 90% interval taken. Wild-type eyes should have very well-defined distributions with small widths, whereas genotypes presenting a high degree of distortion, such as those with fused or warped ommatidia, will have wider distributions.

A distortion coefficient  $\Delta_R$  is calculated for the distribution of roundness for each image. These distortion coefficients are collected into overarching distributions of genotypic variability. In this way, the variation in roundness can be compared between two genotypes by comparing distributions of distortion coefficients between the genotypes.

No parametric form is assumed for the distribution of distortion coefficients. Comparisons between genotypes are made using the Mann-Whitney test (Corder and Foreman, 2009), a non-parametric statistical test with the null hypothesis that the two independent samples being compared come from the same distribution. This significance test allows one to make a qualified judgment as to whether certain differences between genotype are present. In addition, due to the number of gene interactions that were tested, the  $p$ -value was assessed against a multiple comparison Bonferroni-corrected threshold (Salkind, 2007), where the number of tests was equal to the number of possible pairs of genotypes considered – in this case, four genotypes are tested, totalling seven pairwise comparisons.

The results of these comparisons provide an estimate of dissimilarity between two genotypes. If, instead, one genotype were to be compared with an ideal set of measurements of distances, angles, and roundness measures, this test would provide an assessment of how much the genotype of interest deviates from the norm. By choosing a control genotype, an approximation of the ideal distributions of distortion coefficients, incorporating measurement error, is made, which can be compared against the distortion coefficient distributions from a genotype of interest. It is then possible to obtain a quantitative measure of the distortion of a genotype, if it is statistically significant.

**Acknowledgments:** This work was supported by the EPSRC (grant EP/E501311/1). JA was supported by the HEFCE / EPSRC CRiSM grant. CL-A was an Alzheimer's Research Trust PhD scholar.

**References:** Ambegaokar, S.S., and G.R. Jackson 2010, *Genetics* 186: 435-442; Basu, M., 2002, *IEEE Trans. Sys. Man Cyber. C* 32: 252-260; Bilen, J., and N.M. Bonini 2005, *Annu. Rev. Genet.* 39: 53-171; Bourouis, M., 2002, *Genesis* 34(1-2): 99-102; Brand, A.H., and N. Perrimon 1993, *Devel.* 118: 401-415; Buckingham, S.D., and D.B. Sattelle 2008, *Invert. Neurosci.* 8: 121-131; Chatterjee, S., T.K. Sang, G.M. Lawless, and G.R. Jackson 2009, *Human Mol. Genet.* 18: 164-177; Corder, G.W., and D.I. Foreman 2009, *Nonparametric Statistics for Non-Statisticians: A Step-By-Step Approach*, Wiley; Ellis, M.C., E.M. O'Neil, and G.M. Rubin 1993, *Devel.* 119: 855-865; Gonzalez, R.C., and R.E. Woods 1992, *Digital Image Processing*, Addison-Wesley; Gonzalez, R.C., R.E. Woods, and S.L. Eddins 2004, *Digital Image Processing Using MATLAB*, Pearson Prentice Hall; Iijima-Ando, K., and K. Iijima 2010, *Brain Struct. Funct.* 214: 245-262; Johnson, R.I., and R.L. Cagan 2009, *PLOS ONE* 4: e7008; Lu, B., and H. Vogel 2009, *Annu. Rev. Pathol.* 4: 315-342; Maynard, P., 2005, *Drawing Distinctions: The Varieties of Graphic Expression*, Cornell University Press; Moses, K., 2002, *Drosophila Eye Development*, Springer; Muraro, N.I., and K.G. Moffat 2006, *J. Neurobiol.* 66: 1338-1353; Pandey, U.B., Z. Nie, Y. Batlevi, B.A. McCray, G.P. Ritson, N.B. Nedelsky, S.L. Schwartz, N.A. DiProspero, M.A. Knight, O. Schuldiner, R. Padmanabhan, M. Hild, D.L. Berry, D. Garza, C.C. Hubbert, T.P. Yao, E.H. Baehrecke, and J.P. Taylor 2007, *Nature* 447: 859-863; Salkind, N., 2007, *Encyclopedia of Measurement and Statistics*, SAGE; Sobel, I, at a talk at the Stanford Artificial Project in 1968, unpublished but often cited, orig. in *Pattern Classification and Scene Analysis*, Duda, R., and P. Hart, John Wiley and Sons, 271-272; St. Johnston, D., 2002, *Nat. Rev. Genet.* 3: 176-188; Verbeek, P.W., and L.J. van Vliet 1994, *IEEE Trans. Patt. Anal. Mach. Intell.* 16: 726-733; Wittmann, C.W., M.F. Wszolek, J.M. Shulman, P. Salvaterra, J. Lewis, M Hutton, and M.B. Feany 2001, *Science* 293: 711-714; Zhang, L., Q.G. Wang, and J.P. Qi 2006, 'Research based on fuzzy algorithm of cancer cells in pleural fluid microscopic images recognition', *International Conference on Intelligent Information Hiding and Multimedia Signal Processing*, pp. 211-214; Zuiderveld, K., 1994, 'Contrast-Limited Adaptive Histogram Equalization', In: *Graphic Gems IV*, (Heckbert, P.S., ed.), San Diego: Academic Press Professional.

### **Neuroprotective activity of Curcumin against paraquat induced oxidative stress markers in *Drosophila melanogaster*.**



**Ramakrishna, M.K.<sup>1</sup>, C.G. Darshan Raj<sup>2</sup>, L. Kusuma<sup>1</sup>, B.K. Sarojini<sup>2</sup>, and S.R. Ramesh<sup>1</sup>.** <sup>1</sup>Drosophila Stock Centre, DST Unit on Evolution and Genetics, Department of Studies in Zoology, University of Mysore, Manasagangotri, Mysore-570 006 Karnataka; <sup>2</sup>Department of Chemistry, P. A. College of Engineering, Nadupadavu,

Mangalore – 574 153, Karnataka, India.

### **Introduction**

Neurodegenerative disorders are an important source of morbidity and suffering for mankind. The roles of free-radical-mediated oxidative injury in acute insults to the nervous system including stroke or trauma, as well as in chronic neurodegenerative disorders, are being increasingly recognized. It is known that oxygen is an essential molecule for survival of the majority of living